J Appl Electrochem (2012) 42:727–735
DOI 10.1007/s10800-012-0459-4

ORIGINAL PAPER

Electrochemical performance of $La_{0.75}Sr_{0.25}Cr_{0.9}M_{0.1}O_3$ perovskites as SOFC anodes in CO/CO_2 mixtures

F. M. Sapountzi · S. Brosda · K. M. Papazisi · S. P. Balomenou · D. Tsiplakides

Received: 20 February 2012 / Accepted: 21 July 2012 / Published online: 8 August 2012

Abstract The performance of $La_{0.75}Sr_{0.25}Cr_{0.9}M_{0.1}O_3$ (M = Mn, Fe, Co, and Ni) perovskitic materials as anodes was studied for a CO-fueled solid oxide fuel cell. The electrocatalytic performance and the tolerance to carbon deposition were investigated, while electrochemical characterization was carried out via AC impedance spectroscopy and cyclic voltammetry. The $La_{0.75}Sr_{0.25}Cr_{0.9}Fe_{0.1}O_3$ perovskite showed the best anode performance at temperatures above 900 °C; while at temperatures below 900 °C, the best performance was achieved with the $La_{0.75}Sr_{0.25}Cr_{0.9}Co_{0.1}O_3$ material. AC impedance spectroscopy was used for a semi-quantitative analysis of the LSC-$M_{0.1}$ anodes performance in view of total cell and charge transfer resistance. All anode materials exhibit high electronic conductivity and presumably do not substantially contribute to the overall cell resistance and concomitant ohmic losses.

Keywords SOFC · CO · Perovskites · Anode · Coke formation · AC impedance · Cyclic voltammetry

F. M. Sapountzi (✉) · S. Brosda
Department of Chemical Engineering, University of Patras, Caratheodory 1 Str., 26504 Patras, Greece
e-mail: fenia@chemeng.upatras.gr

K. M. Papazisi · S. P. Balomenou · D. Tsiplakides
CPERI/CERTH, 6th km Charilaou-Thermi Rd., 57001 Thessaloniki, Greece

K. M. Papazisi
Department of Chemical Engineering, Aristotle University of Thessaloniki, 54006 Thessaloniki, Greece

D. Tsiplakides
Department of Chemistry, Aristotle University of Thessaloniki, 54124 Thessaloniki, Greece

1 Introduction

Solid oxide fuel cells (SOFCs) are efficient devices that convert chemical fuels directly into electrical power [1, 2]. The high operating temperature of SOFCs (600–1,000 °C) gives them a number of benefits, such as (a) the possibility of using hydrocarbons directly as fuels without the need of external reformers which allows flexibility in the choice of fuel, and (b) the production of heat as by-product in addition to the electrical power [1, 2]. Unlike low temperature fuel cells, no precious metals are needed as catalysts due to the fast kinetics at elevated operating temperatures. In comparison to polymer electrolyte membrane fuel cells, carbon monoxide does not poison the anode of a SOFC, on the contrary, CO can be used as a fuel [2, 3]. The development of CO-fueled SOFCs is of great interest for space applications, taking into account that the Martian atmosphere consists of 96 % CO_2, which can be decomposed via electrolysis into CO and oxygen [4] to supply them to the anode and the cathode [5], respectively. Recent studies concerning the use of a regenerative SOFC in Mars have shown promising results [6].

The main problem related to the direct use of hydrocarbons or CO in a SOFC unit is coke formation leading to contamination and thus to decreased life time of the anode [7]. Poisoning reactions, which are responsible for the anode-catalyst deactivation due to carbon deposition, are the decomposition/cracking of hydrocarbons, e.g., CH_4, (1) and the Boudouard reaction (2)

$$CH_4 \rightarrow C + 2H_2 \quad (1)$$

$$2CO \rightarrow C + CO_2 \quad (2)$$

The most commonly used anode material for SOFCs is the Ni/YSZ cermet, which exhibits excellent catalytic

performance for fuel oxidation and high electronic conductivity. However, the use of the Ni/YSZ cermet-anode has some drawbacks, such as its sensitivity to sulfur poisoning and to carbon deposition and its poor redox stability [8–15].

Perovskite oxides have been studied as alternative anode materials due to their excellent stability under both oxidizing and reducing conditions [14–16]. The mixed ionic-electronic conductivity of such oxides can extend the reaction zone from the triple phase boundaries to the whole electrode/gas interface, thus minimizing the electrode overpotential [14, 15]. Oxides generally show a better tolerance to carbon deposition and sulfur poisoning and sustain redox cycling with less morphological changes [15]. Moreover, oxides have very high melting temperatures and relatively low surface energies, and thus tend to be more resistant to sintering compared to metals [17].

Up to now, $LaCrO_3$-based materials have been primarily investigated as interconnect materials for SOFCs [18, 19]; however, they are also potential anode materials for SOFCs due to their relatively good stability in both reducing and oxidizing atmospheres at high temperatures [20]. The reported polarization resistance using these materials is quite high for sufficient SOFC operation although significant improvements have been achieved by low-level doping of the B-site. The introduction of transition elements into the B-site of $La_{1-x}Sr_xCr_{1-y}M_yO_3$ (M = Mn, Fe, Co, and Ni) has significantly improved their catalytic properties [20–25].

In a recent study [5], a series of $La_{0.75}Sr_{0.25}Cr_{0.9}M_{0.1}O_3$ (M = Mn, Fe, Co, and Ni) perovskite materials was synthesized by a modified citrate sol–gel route and deposited by air-pressurized spraying on YSZ (yttria-stabilized zirconia), and subsequently operated as anodes for a CO-fueled SOFC, revealing that the most promising material is $La_{0.75}Sr_{0.25}Cr_{0.9}Fe_{0.1}O_3$.

The aim of the present study was to examine in more detail the electrocatalytic and electrochemical performance as well as the tolerance to coke deposition of the $La_{0.75}Sr_{0.25}Cr_{0.9}M_{0.1}O_3$ (M = Mn, Fe, Co, and Ni) anode materials series in a CO-fueled SOFC. In situ electrochemical impedance spectroscopy (EIS) and cyclic voltammetry (CV) in parallel to electrocatalytic investigations have been carried out to gain semi-quantitative insight on the total cell and charge transfer resistance.

2 Experimental

2.1 Materials synthesis and preparation

A series of $La_{0.75}Sr_{0.25}Cr_{0.9}M_{0.1}O_3$ (M = Mn, Fe, Co, and Ni) perovskite-type compounds, hereafter denoted as LSC-$M_{0.1}$, were synthesized by a modified citrate/sol–gel route [26, 27] as described in detail elsewhere [5].

The powders were used as anodes for a series of button cells [5] developed on YSZ solid electrolyte disk substrates (Dynamic Ceramic, Technox 802) with a thickness of 1.6 ± 0.05 mm and a diameter of 20 mm. The LSC-$M_{0.1}$ anodes and commercially available LSM cathode ink (NexTech Materials) were deposited on the opposite sides of the YSZ pellets by air-pressurized spraying. In this process, a mixture of the perovskite powder dissolved in a terpineol-based ink vehicle (Fuel Cell Materials) was sprayed through a nozzle (Budger Air-brush Model 150) for 140 s on the YSZ substrate. The resulting electrodes, after calcination and sintering at 1,100 °C, had a thickness of 21 ± 4 μm and a geometric surface area of 1.55 cm^2. The average catalyst loading for all samples was 10.5 mg cm^{-2}.

2.2 Electrocatalytic and electrochemical measurements

The electrocatalytic and electrochemical testing of the button cells was carried out in a SOFC reactor with anode volume of 50 cm^3, shown schematically in Fig. 1. The button cells were positioned on the top of an Al_2O_3 tube. A gold gasket of 1 mm thickness was placed between the button cell and the alumina tube. A stepwise thermal treatment was followed with heating up to 1,000 °C with a rate of 8 K min^{-1}, then heating from 1,000 to 1,055 °C with a rate of 2 K min^{-1} and finally annealing at 1,055 °C for 2 h to insure efficient sealing of the anode

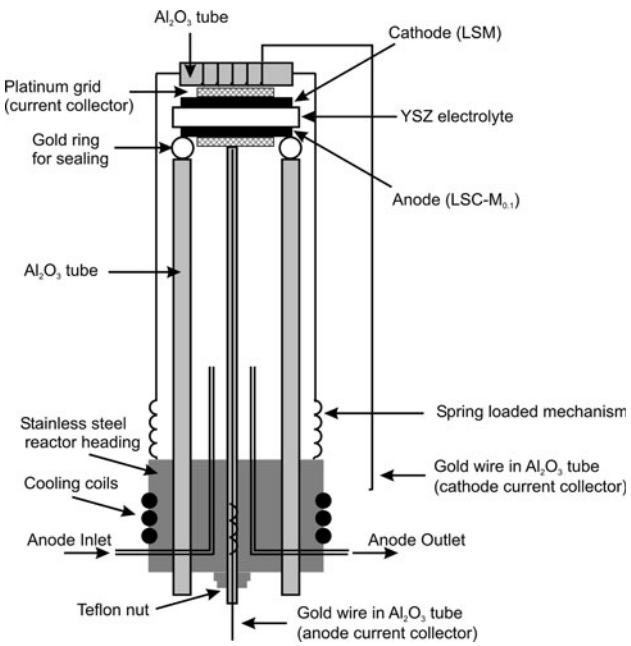

Fig. 1 Schematic representation of the experimental setup for the electrocatalytic and electrochemical testing of the button cells

compartment. Platinum gauzes (52 mesh) pressed on both anode and cathode electrodes and gold wires (Alfa Aesar, 0.5 mm diameter) were used as current collectors. An Al_2O_3 ceramic holder was used to keep the sample attached to the Al_2O_3 tube by a spring loaded mechanism. The operating temperature was monitored via a thermocouple (type K) in contact with the sample.

The anode was fed with a CO/CO_2 gas mixture (0.9 % CO/0.1 % CO_2 with He as balance). The specific fuel selection is dictated by the underlying research aim toward the development of CO-fueled SOFCs for space applications and particularly for the Martian atmosphere. In view of this, the gas mixture used is a diluted simulation of the thin Martian atmosphere; taking into account the difference in atmospheric pressure conditions (the atmospheric pressure at the surface of the planet is about 1/100th of that of Earth's, i.e. 0.15 psi). The total gas flow rate at the anode side was 300 cm^3 (STP) min^{-1}. The cathodic compartment was supplied with a gas mixture of 20 % O_2 diluted in He and the total gas flow rate at the cathode side was 70 cm^3 (STP) min^{-1}.

Gas flow rates were regulated using Brooks mass flow controllers connected to a 4-channel Brooks control box (model 5878). Gas analysis was performed by on-line gas-chromatography (Hewlett Packard 5890 Series II), utilizing a thermal conductivity detector (TCD) and equipped with two columns, a molecular sieve 5A (for the detection of O_2, N_2 and CO) and a Porapak Q column (for the detection of CO_2). TCD signals were integrated and recorded on-line by the use of a Hewlett Packard integrator (model 3395). An infrared CO_2 analyzer (Rosemount Binos 100) was used for continuous monitoring of the CO_2 concentration in the effluent stream.

Currents and potentials were applied by means of a Solartron electrochemical interface 1286. AC impedance spectra were obtained both under open-circuit conditions and under cell polarization using a Solartron SI 1255 frequency response analyzer and a 1286 electrochemical interface. Impedance spectroscopy data were collected at the reaction steady-state and in the frequency range between 10^6 and 0.01 Hz using an AC stimulus amplitude of 20–30 mV.

Experiments were always carried out with increasing temperature and the polarization data were obtained potentiostatically with gradual polarization from the open-circuit potential toward short-circuiting (which corresponds to the maximum current). The cell was always kept under polarization for 10–15 min to reach steady-state in current.

Owing to the imperfection in sealing, there was a consistent leak in the anode compartment in all our measurements. This leak was present and stable and was not affected by cooling or heating procedures, but resulted in the presence of a small oxygen concentration in the anode compartment. This was also manifested by the open-circuit potential, which deviated from the theoretic Nernst value.

3 Results and discussion

3.1 Performance of the LSC-$M_{0.1}$ anodes during fuel cell operation

The performance of the LSC-$M_{0.1}$ anodes was evaluated in terms of electrocatalytic activity and tolerance to carbon deposition during CO-fueled operation of the button cells.

The electrochemical reactions which take place during fuel cell operation are

$$\text{Cathode}: {}^{1}/_{2}\ O_2 + 2e^- \rightarrow O^{2-} \quad (3)$$

$$\text{Anode}: CO + O^{2-} \rightarrow CO_2 + 2e^- \quad (4)$$

The electrocatalytic rate of CO_2 production, r_{CO_2}, is defined by the equation:

$$r_{CO_2} = F\left(y^{\text{out}}_{CO_2} - y^{\text{in}}_{CO_2}\right), \quad (5)$$

where F is the volumetric flowrate (mol s^{-1}), $y^{\text{out}}_{CO_2}$ is the outlet CO_2 molar fraction, and $y^{\text{in}}_{CO_2}$ is the inlet CO_2 molar fraction.

Figure 2 shows an Arrhenius-type plot of the electrocatalytic rate of CO_2 production at $U_{\text{cell}} = 0$ V versus the inverse of temperature. The values of the activation energy for the electrochemical oxidation of CO were calculated

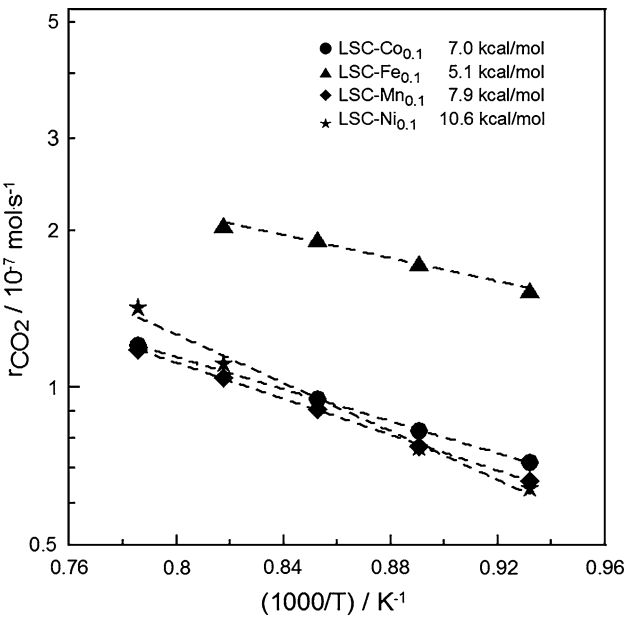

Fig. 2 Electrocatalytic rate of carbon dioxide production (r_{CO_2}) versus the inverse of temperature ($1/T$) at $U_{\text{cell}} = 0$ V. The corresponding activation energies for the electrochemical oxidation of CO are shown. Anode feed: 0.9 % CO/0.1 % CO_2

from the slopes and were found to vary roughly between 5.1 and 10.6 kcal mol^{-1}. The highest rate at all temperatures as well as the lowest value of 5.1 kcal mol^{-1} was obtained with the LSC-$Fe_{0.1}$ anode, indicating that among the tested electrodes LSC-$Fe_{0.1}$ is the most active electrode for electrochemically oxidizing CO, while the less active electrode is LSC-$Ni_{0.1}$.

In general, strontium-doped lanthanum chromites do not suffer from carbon deposition [28] and thus they are considered as potential anodes for direct hydrocarbon (e.g., methane) oxidation in SOFC [29, 30]. In order to ascertain whether carbon deposition takes place on the LSC-$M_{0.1}$ anodes, the carbon mass balance was followed during fuel cell operation in a CO–CO_2 mixture. For the LSC-$M_{0.1}$ anodes, the electrocatalytic rate of CO consumption, $-r_{CO}$, was cross-plotted versus the electrocatalytic rate of CO_2 production, r_{CO_2}, over the entire temperature range, as shown in Fig. 3a–c. The dashed lines in the figures correspond to the stoichiometric conversion of CO in CO_2. As shown in Fig. 3a, the experimental values of the electrocatalytic rates for the LSC-$Fe_{0.1}$ and LSC-$Co_{0.1}$ anodes fall very close to the dashed line, indicating that both samples exhibit a high tolerance to coke deposition. The data obtained with the LSC-$Ni_{0.1}$ and LSC-$Mn_{0.1}$ anodes deviate slightly from the dashed line (stoichiometric line), indicating that most likely carbon deposition has taken place on these electrodes. The rate of carbon deposition on the LSC-$Ni_{0.1}$ (Fig. 3b) and LSC-$Mn_{0.1}$ (Fig. 3c) anodes can be estimated via extrapolation of the linear fit (shown with the dotted lines in Fig. 3b, c) to the zero value of r_{CO_2}. For the LSC-$Ni_{0.1}$ and LSC-$Mn_{0.1}$ anodes,

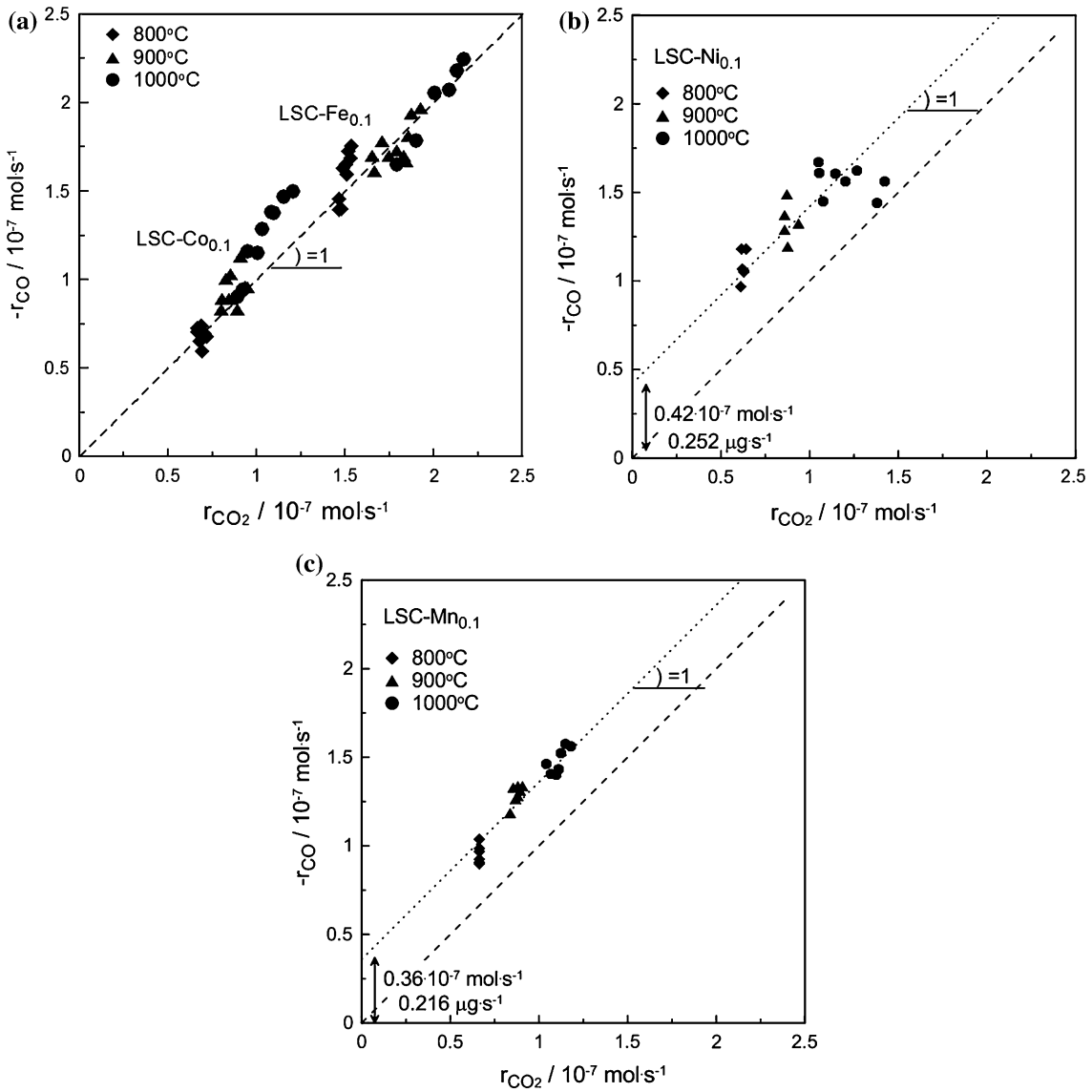

Fig. 3 Electrocatalytic rate of CO consumption ($-r_{CO}$) versus the rate of CO_2 production (r_{CO_2}) for **a** LSC-$Fe_{0.1}$, LSC-$Co_{0.1}$, **b** LSC-$Ni_{0.1}$ and **c** LSC-$Mn_{0.1}$. The *dashed lines* correspond to the stoichiometric conversion of CO in CO_2. Anode feed: 0.9 % CO/0.1 % CO_2

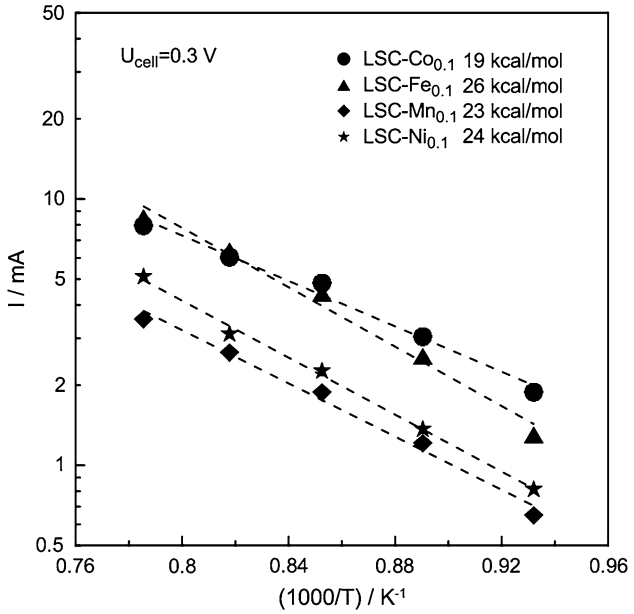

Fig. 4 Effect of inverted temperature on the cell current obtained under polarization of $U_{cell} = 0.3$ V. Anode feed: 0.9 % CO/0.1 % CO_2

carbon deposition rate values of roughly 0.252 and 0.216 μg s^{-1}, respectively, were estimated. In order to confirm carbon formation on the anode electrodes, temperature programed oxidation (TPO) experiments were carried out after the exposure of anodes to the CO/CO_2 reaction mixture. For the TPO experiments, the cell was cooled to 25 °C and 5.6 kPa O_2 in He balance was supplied to the anode. The cell was heated with a heating rate of 5 °C min^{-1} from room temperature to 750 °C, while the CO_2 concentration was continuously monitored. In none of the cases a measurable concentration of CO_2 has been detected, indicating that if there is any carbon formation this corresponds to non-detectable traces, below the sensitivity level of our TPO equipment. This is in agreement with previous study of the LSC-$Fe_{0.1}$ anode material under similar conditions (CO/CO_2 fuel and temperature range), which showed the absence of massive carbon deposition after prolonged SOFC testing [5].

Figure 4 shows, in the form of Arrhenius plots, the effect of temperature on the cell current obtained under polarization of $U_{cell} = 0.3$ V. The LSC-$Fe_{0.1}$ and LSC-$Co_{0.1}$ anodes exhibited the best performance since the current and corresponding power output values at $U_{cell} = 0.3$ V were higher for these electrodes. The activation energies, calculated from the slopes of Fig. 4 and corresponding to the overall cell resistances, vary between 19 and 26 kcal mol^{-1}, which are in the same order of magnitude with the reported values in the literature by Filal et al. [31] for YSZ bulk conductivity.

Obtained currents are relatively small in comparison to the state of the art Ni-YSZ cermet electrodes partly as a result of a non-optimized cell structure in terms of use of thick electrolyte, anode, and cathode microstructure. The utilization of thin electrolyte substrates, in the order of a few micrometer, and the mixing of anode material with YSZ, to form a cermet, would decrease electrode polarization and therefore increase cell performance. Furthermore, the highly diluted fuel used reduces the electrocatalytic rate, resulting in the observed low current densities.

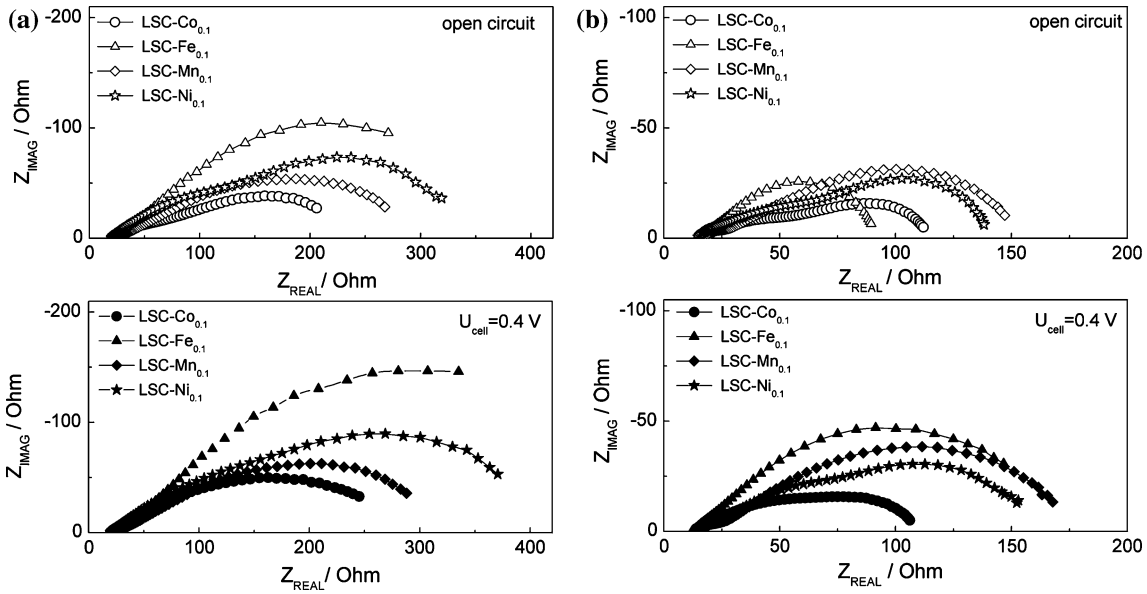

Fig. 5 Electrochemical impedance spectra obtained at **a** 800 and **b** 900 °C, both under open-circuit conditions and under polarization of $U_{cell} = 0.4$ V. Anode feed: 0.9 % CO/0.1 % CO_2

3.2 AC impedance spectroscopy

EIS was used for a semi-quantitative analysis of the LSC-$M_{0.1}$ anodes' performance in view of total cell and charge transfer resistance. Since the cathode electrode and the electrolyte are the same for all button cells, the absence of a reference electrode does not prevent one from having a qualitative overview of the similarities and differences in performance. The analysis was carried out during fuel cell operation with CO/CO_2 supply to the anode (0.9 % CO/0.1 % CO_2) in the temperature range of 800–1,000 °C. Impedance diagrams were recorded both under open-circuit conditions and under polarization of $U_{cell} = 0.4$ V.

Figure 5 shows EIS results obtained at 800 °C (Fig. 5a) and 900 °C (Fig. 5b), both under open-circuit conditions (top part of Fig. 5) and under polarization of $U_{cell} = 0.4$ V (bottom part of Fig. 5). For the Co-, Mn-, and Ni-doped samples, the AC impedance spectra consist of at least two arcs at both temperatures, both at open and closed circuit conditions. The first one at high frequencies (10^6–10^5 Hz) is generally attributed to the bulk and interfacial relaxation processes of the electrolyte (YSZ) and the electrodes, while the second one at low frequencies (10–0.01 Hz) is attributed to the polarization phenomena. The high frequency arc, and thus the overall cell resistance, is not strongly affected by the temperature (within the range of 800–900 °C), while the low frequency arc is expanded with decreasing temperature. The polarization at 0.4 V affects only slightly the high frequency range of the impedance response; while at low frequencies, the polarization resistance increases for all samples with both temperatures presented in Fig. 5a, b. This behavior cannot be attributed to carbon deposition since the effect of carbon deposition, if any, would be less pronounced under polarization. In principle, it could be attributed to polarization-induced changes in the perovskite material, i.e., changes in the stoichiometry and number of oxygen ion vacancies [32].

The impedance data were roughly fitted to an equivalent $R_{cell}(R_1C_1)(R_2C_2)$ electrical circuit by means of the ZView software. The RC impedance response is, for all cases of this study, the equivalent circuit with the fewest and simplest possible fundamental elements. According to Vernoux [33], similar impedance characteristics were observed using lanthanum chromites as anodes for SOFCs working under CO/CO_2 mixtures.

The cell resistance, obtained from the high frequency intersect with the Z_{real}-axis, is in the order of 10 Ω and is only slightly affected by the temperature showing highest values at the lowest temperature, as expected. Assuming that the conductance of the YSZ electrolyte is 0.008–0.01 S cm^{-1} at temperatures of 800–1,000 °C [34], the resistance of the 1.6 mm electrolyte layer should be approximately 5–6 Ω, which is in good agreement with the observed experimental values. Hence, this is an indication that the tested perovskite electrodes have sufficiently high conductivity, and thus do not substantially contribute to the overall cell ohmic resistance.

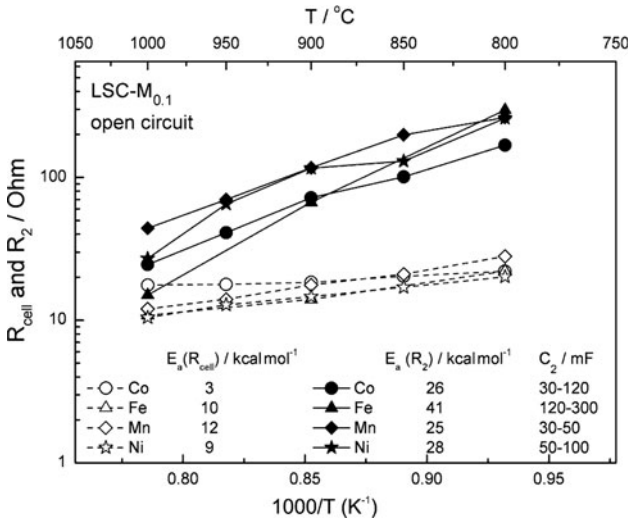

Fig. 6 Cell resistance (R_{cell}), *open symbols*, and charge transfer resistance (R_2), *closed symbols*, as a function of the inverse of temperature. The corresponding activation energies and cell capacitance (C_2) are shown in the *in-set* table. Anode feed: 0.9 % CO/0.1 % CO_2

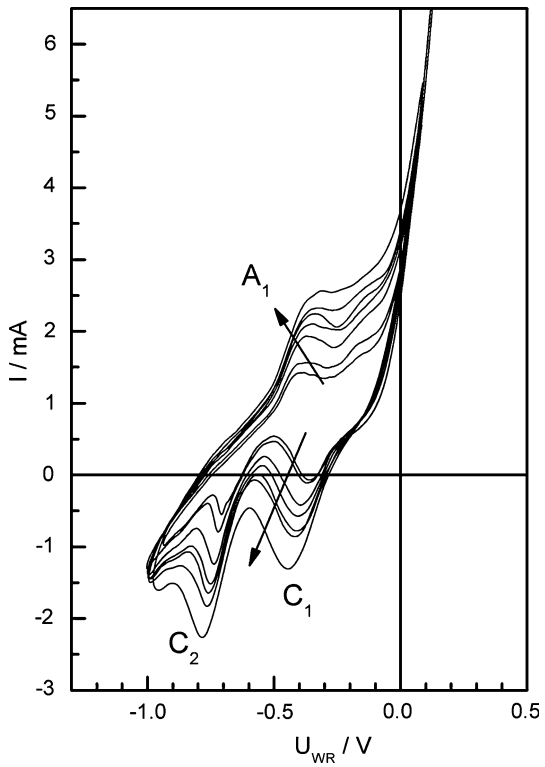

Fig. 7 Cyclic voltammograms of LSC-$Fe_{0.1}$ anode obtained at the three-electrode button cell under CO/CO_2 supply (0.9 % CO/0.1 % CO_2) at 800 °C. *Arrow* shows the order of increasing scan rate: 20, 30, 50, 60, 70, 80, and 100 mV/s

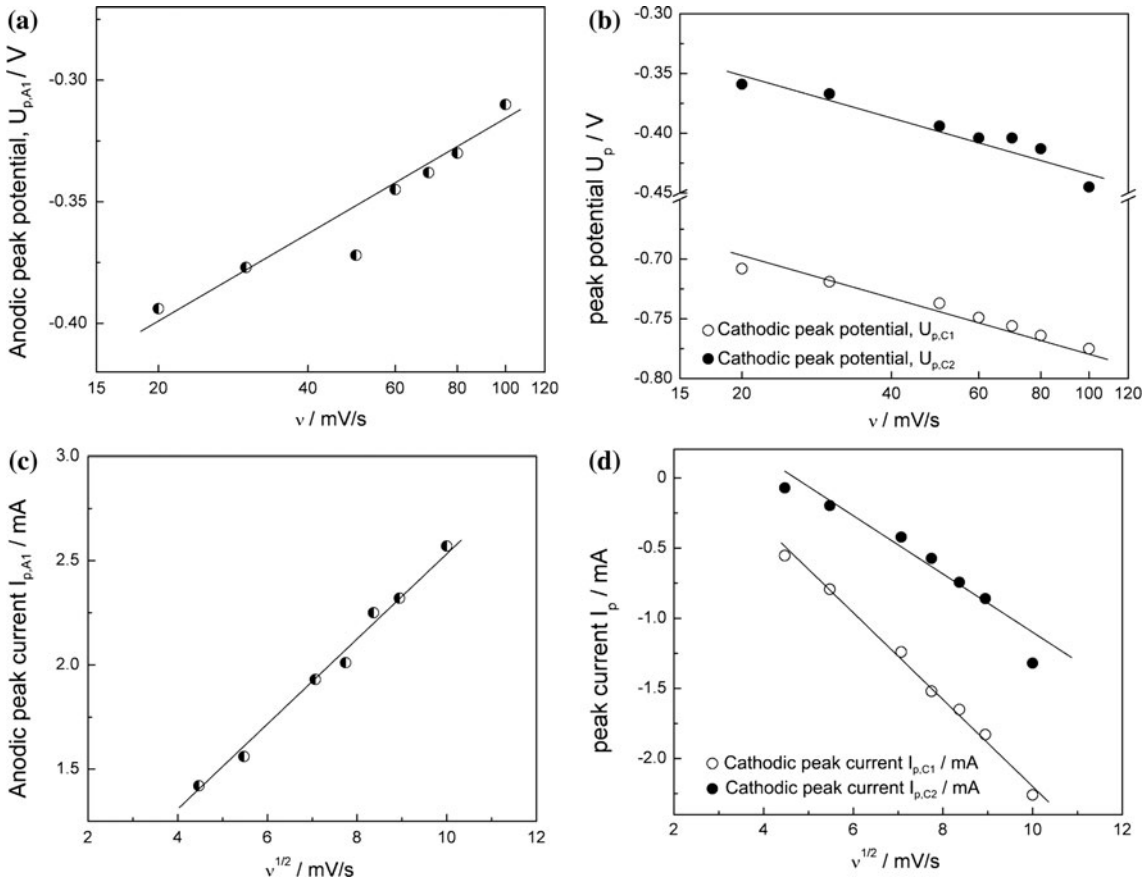

Fig. 8 Effect of scan rate, v, on the anodic (**a**) and cathodic (**b**) peak potentials. Effect of the square route of scan rate, $v^{1/2}$, on the anodic (**c**) and cathodic (**d**) peak currents. Conditions as in Fig. 7

The dependence of the cell resistance, R_{cell}, and charge transfer resistance, R_2, on the inverse of temperature is shown in Fig. 6, for open-circuit conditions. The inset table in Fig. 6 presents a comparison for all samples regarding the activation energy for the ohmic resistance, R_{cell}, and for the charge transfer processes, as well as the concomitant capacitance C_2, under open-circuit conditions. Very similar values were found for the activation energies for R_{cell} and R_2 under polarization of 0.4 V. The corresponding values of the activation energy for R_{cell} were in the range of 3–11 kcal mol^{-1} (Fig. 6).

As shown in Fig. 6, the button cell with the LSC-$Fe_{0.1}$ anode exhibited the best impedance characteristics (lowest R_2) at temperatures above 900 °C and open-circuit conditions, while below 900 °C the button cell with the LSC-$Co_{0.1}$ anode had the lowest R_2. The superior performance of LSC-$Fe_{0.1}$ anode was also observed under 0.4 V at the highest temperature (1,000 °C). The activation energy for the low frequency process, R_2, was estimated between 25 and 41 kcal mol^{-1} under open-circuit conditions and between 21 and 47 kcal mol^{-1} under $U_{cell} = 0.4$ V. The high values of the activation energy are indicative of a thermally activated process.

3.3 Cyclic voltammetry

CV experiments for all anode samples were initially carried out in two electrode configuration (anode–cathode) scanning the potential between −1 and 0.1 V at scan rates of 20–120 mV s^{-1} under the CO/CO_2 reaction mixture (0.9 % CO/0.1 % CO_2) and in the temperature range 800–1,000 °C. Anodic and cathodic peaks were observed in the voltammograms only for temperatures below 900 °C and only for the case of the LSC-$Fe_{0.1}$ anode. In order to further investigate the behavior of this sample, a Pt reference electrode was deposited next to the cathode (counter) electrode.

Figure 7 shows the effect of scan rate on the voltammograms obtained with the three-electrode button cell with LSC-$Fe_{0.1}$ anode, under CO/CO_2 supply at 800 °C. These voltammograms correspond to the 10th scan. Two cathodic peaks (denoted in Fig. 7 as C_1 and C_2 and one peak (denoted in Fig. 7 as A_1) are observed. The cathodic peaks are shifted to lower potentials with increasing scan rate; the anodic peaks are shifted to higher potentials with increasing scan rate, while the absolute value of the peak current, for all the three peaks evolving, is increased with increased scan rate.

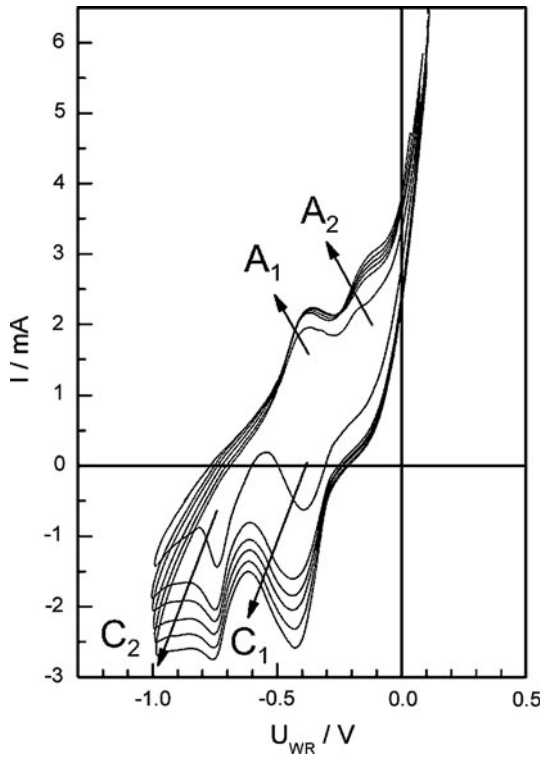

Fig. 9 Cyclic voltammograms of LSC-$Fe_{0.1}$ anode following a polarization at $U_{cell} = 0$ V for various holding times under CO/CO_2 supply (0.9 % CO/0.1 % CO_2) at 800 °C. *Arrow* shows the order of increasing holding time: 0, 30, 60, 120, 180, and 300 s

Similar peaks have been observed in the cyclic voltammograms by Bebelis et al. [35] using $La_{0.78}Sr_{0.2}FeO_{3-\delta}$ and $La_{0.78}Sr_{0.2}Co_{0.2}Fe_{0.8}O_{3-\delta}$ electrodes interfaced to ceria-doped gadolinium oxide (CGO)/YSZ electrolyte and by Siebert et al. [36] using $La_{0.7}Sr_{0.3}Co_{0.8}Fe_{0.2}O_{3-\delta}$ interfaced to CGO. The observed peaks are probably related to the electrochemical redox process of iron ions [35]. Two such reduction processes occur at potentials of −0.8 and −0.4 V and they may correspond to the reduction of Fe^{+4} and Fe^{+3}, respectively.

Figure 8a–d shows the effect of scan rate, v, on the peak potential and peak current obtained from the cyclic voltammograms of Fig. 7. A linear dependence between the peak current, I_p, and $v^{1/2}$ is found. Both for the anodic and the cathodic peaks, the peak potential, U_p, varies linearly with the logarithm of the scan rate, indicating that the electrochemical system is irreversible [35, 37].

When the electrode potential is higher than 0 V, a significant evolution of current is observed (Fig. 7) due to the oxygen evolution taking place at the anode. In the backward (anodic) scan, the observed peak can correspond to the reoxidation of the Fe^{+3} or Fe^{+2} ions which have been formed during the forward (cathodic) scan. However, it is not clear whether the peak A_1 corresponds to reoxidation of the species formed during C_1 or C_2. The absence of a second peak during the anodic scan could be related with the gaseous oxygen generated during current evolution. If the iron ions have high redox stability, this oxygen could competitively participate in the oxidation of the reduced iron ions (chemical re-oxidation) and thus dominate over the electrochemical process [35, 38].

In order to investigate the stability of Fe^{3+} and Fe^{4+} under oxygen evolution, a pretreatment of the cell was carried out at a polarization of +0.1 V for different holding times. Then, at $T = 800$ °C, the response of the current was followed during sweeping the potential from +0.1 V down to the potential of −1 V and then back to +0.1 V with a constant sweep rate of 100 mV s^{-1}. As presented in Fig. 9, after anodic polarization, an indication of a second peak A_2 (shoulder) appears in the voltammograms at lower absolute potential values (at the right of A_1). This implies that under oxygen evolution, the stability of Fe^{3+} and Fe^{4+} is decreased; during the anodic scan, the electrochemical reaction becomes also competitive.

4 Conclusions

$La_{0.75}Sr_{0.25}Cr_{0.9}M_{0.1}O_3$ (M = Mn, Fe, Co, and Ni) perovskite-type compounds were tested and operated as anodes in a button cell-type SOFC using YSZ as solid electrolyte and commercial LSM as cathode. The cells were studied with a CO/CO_2 mixture (0.9 % CO/0.1 % CO_2) fed to the anode and air to the cathode in the temperature range of 800–1,000 °C. The $La_{0.75}Sr_{0.25}Cr_{0.9}Fe_{0.1}O_3$ electrocatalyst showed the best performance at temperatures above 900 °C; while at temperatures below 900 °C, the best performance was achieved with the sample $La_{0.75}Sr_{0.25}Cr_{0.9}Co_{0.1}O_3$. All anodes exhibited high tolerance to carbon deposition. Furthermore, all anode materials exhibited high electronic conductivity, and thus do not substantially contribute to the overall cell resistance and concomitant Ohmic losses. The activation energy for the charge transfer resistance obtained with EIS is in the order of 20–47 kcal mol^{-1}.

Acknowledgments Partial financial support from the European Space Agency (ESA) is gratefully acknowledged. We wish to thank Prof. Constantinos Vayenas for providing helpful discussion and motivation of the present study.

References

1. Douvartzides SL, Coutelieris FA, Demin AK, Tsiakaras PE (2004) Electricity from ethanol fed SOFCs: the expectations for sustainable development and technological benefits. Int J Hydrog Energy 29:375–379. doi:10.1016/S0360-3199(03)00047-8
2. Singhal SC, Kendal K (2003) High temperature solid oxide fuel cells: fundamentals, design and applications. Elsevier, UK

3. Escudero MJ, Irvine JTS, Daza L (2009) Development of anode material based on La-substituted $SrTiO_3$ perovskites doped with manganese and/or gallium for SOFC. J Power Sources 192:43–50. doi:10.1016/j.jpowsour.2008.11.132
4. Bidrawn F, Kim G, Corre G, Irvine JTS, Vohs JM, Gorte RJ (2008) Efficient reduction of CO_2 in a solid oxide electrolyzer. Electrochem Solid State Lett 11:B167–B170. doi:10.1149/1.2943664
5. Papazisi KM, Balomenou S, Tsiplakides D (2010) Synthesis and characterization of $La_{0.75}Sr_{0.25}Cr_{0.9}M_{0.1}O_3$ perovskites as anodes for CO-fueled solid oxide fuel cells. J Appl Electochem 40:1875–1881. doi:10.1007/s10800-010-0150-6
6. Pipoli T, Besenhard JO, Schautz M (2002) In situ production of fuel and oxidant for a small solid oxide fuel cell on Mars. In: Wilson A (ed) Sixth European Space Power Conference (ESPC). ESA Publications Division (Noordwijk), Porto
7. Tsang SC, Claridge JB, Green MLH (1995) Recent advances in the conversion of methane to synthesis gas. Catal Today 23:3–15. doi:10.1016/0920-5861(94)00080-L
8. Deleebeeck L, Fournier JL, Birss V (2010) Comparison of Sr-doped and Sr-free $La_{1-x}Sr_xMn_{0.5}Cr_{0.5}O_{3\pm\delta}$ SOFC Anodes. Solid State Ion 181:1229–1237. doi:10.1016/j.ssi.2010.05.027
9. Tao S, Irvine JTS (2004) Discovery and characterization of novel oxide anodes for solid oxide fuel cells. Chem Rec 4:83–95. doi:10.1002/tcr.20003
10. Tao S, Irvine JTS (2004) Synthesis and characterization of $La_{0.75}Sr_{0.25}Cr_{0.5}Mn_{0.5}O_{3-\delta}$, a redox-stable, efficient perovskite anode for SOFCs. J Electrochem Soc 151:A252–A259. doi:10.1149/1.1639161
11. Matsuzaki Y, Yasuda I (2000) The poisoning effect of sulfur-containing impurity gas on a SOFC anode: part I. Dependence on temperature, time, and impurity concentration. Solid State Ion 132:261–269. doi:10.1016/S0167-2738(00)00653-6
12. Steele BCH, Kelly I, Middleton H, Rudkin R (1988) Oxidation of methane in solid state electrochemical reactors. Solid State Ion 28–30:1547–1552. doi:10.1016/0167-2738(88)90417-1
13. Mukundan R, Brosha EL, Garzon FH (2004) Sulfur tolerant anodes for SOFCs. Electrochem Solid State Lett 7:A5–A7. doi:10.1149/1.1627452
14. Sun C, Stimming U (2007) Recent anode advances in solid oxide fuel cells. J Power Sources 171:247–260. doi:10.1016/j.jpowsour.2007.06.086
15. Fu Q, Tietz F, Stover D (2006) Synthesis and electrical conductivity of Sr- and Mn-substituted $LaAlO_3$ as a possible SOFC anode material. Solid State Ion 177:1819–1822. doi:10.1016/j.ssi.2006.03.028
16. Vert VB, Melo FV, Navarrete L, Serra JM (2012) Redox stability and electrochemical study of nickel doped chromites as anodes for H_2/CH_4-fueled solid oxide fuel cells. Appl Catal B 115–116:346–356. doi:10.1016/j.apcatb.2011.12.033
17. McIntosh S, Gorte RJ (2004) Direct hydrocarbon solid oxide fuel cells. Chem Rev 104:4845–4866. doi:10.1021/cr020725g
18. Sundmacher K (2010) Fuel cell engineering: toward the design of efficient electrochemical power plants. Ind Eng Chem Res 49:10159–10182. doi:10.1021/ie100902t
19. Mori M, Hiei Y, Sammes NM (1999) Sintering behavior and mechanism of Sr-doped lanthanum chromites with A site excess composition in air. Solid State Ion 123:103–111. doi:10.1016/S0167-2738(99)00097-1
20. Yokokawa H, Sakai N, Kawada T, Dokiya M (1992) Thermodynamic stabilities of perovskite oxides for electrodes and other electrochemical materials. Solid State Ion 52:43–56. doi:10.1016/0167-2738(92)90090-C
21. Primdahl S, Hansen JR, Grahl-Madsen L, Larsen PH (2001) Sr-doped $LaCrO_3$ anode for solid oxide fuel cells. J Electrochem Soc 148:A74–A81. doi:10.1149/1.1344519
22. Danilovic N, Vincent A, Luo JL, Chuang KT, Hui R, Sanger AR (2010) Correlation of fuel cell anode electrocatalytic and ex situ catalytic activity of perovskites $La_{0.75}Sr_{0.25}Cr_{0.5}X_{0.5}O_{3-\delta}$ (X = Ti, Mn, Fe, Co). Chem Mater 22:957–965. doi:10.1021/cm901875u
23. Zha S, Tsang P, Cheng Z, Liu M (2005) Electrical properties and sulfur tolerance of $La_{0.75}Sr_{0.25}Cr_{1-x}Mn_xO_3$ under anodic conditions. J Solid State Chem 178:1844–1850. doi:10.1016/j.jssc.2005.03.027
24. Sfeir J, Buffat PA, Möckli P, Xanthopoulos N, Vasquez R, Mathieu HJ, van Herle J, Thampi KR (2001) Lanthanum chromite based catalysts for oxidation of methane directly on SOFC anodes. J Catal 202:229–244. doi:10.1006/jcat.2001.3286
25. Sfeir J (2003) $LaCrO_3$-based anodes: stability considerations. J Power Sources 118:276–285. doi:10.1016/S0378-7753(03)00099-5
26. Sfeir J, van Herle J, McEvoy AJ (1999) Stability of calcium substituted lanthanum chromites used as SOFC anodes for methane oxidation. J Eur Ceram Soc 19:897–902. doi:10.1016/S0955-2219(98)00340-9
27. Kong J, Zhang Y, Deng C, Xu J (2009) Synthesis and electrochemical properties of LSM and LSF perovskites as anode materials for high temperature steam electrolysis. J Power Sources 186:485–489. doi:10.1016/j.jpowsour.2008.10.053
28. Fergus JW (2006) Oxide anode materials for solid oxide fuel cells. Solid State Ion 177:1529–1541. doi:10.1016/j.ssi.2006.07.012
29. Vulliet J, Morel B, Laurencin J, Gauthier G, Bianchi L, Giraud S, Henry HY, Lefebvre-Joud F (2003) First results on a (La, Sr)CrO_3 anode fed with methane. Electrochem Soc Proc SOFC VIII, p 803
30. Weston M, Metcalfe IS (1998) $La_{0.6}Sr_{0.4}Co_{0.2}Fe_{0.8}O_3$ as an anode for direct methane activation in SOFCS. Solid State Ion 113–115:247–251. doi:10.1016/S0167-2738(98)00377-4
31. Filal M, Petot C, Chateau C, Carpentier JL (1995) Ionic conductivity of yttrium-doped zirconia and the "composite effect". Solid State Ion 80:27–35. doi:10.1016/0167-2738(95)00137-U
32. Hagen A, Traulsen ML, Kiebach WR, Johansen BS (2012) Spectroelectrochemical cell for in situ studies of solid oxide fuel cells. J Synchrotron Rad 19:400–407. doi:10.1107/S0909049512006760
33. Vernoux P (1997) Lanthanum chromites as an anode material for solid oxide fuel cells. Ionics 3:270–276. doi:10.1007/BF02375628
34. Rickert H (1978) Solid ionic conductors: principles and applications. Angew Chem Int Ed Engl 17:37–46. doi:10.1002/anie.197800371
35. Bebelis S, Kournoutis V, Mai A, Tietz F (2008) Cyclic voltammetry of $La_{0.78}Sr_{0.2}FeO_{3-\delta}$ and $La_{0.78}Sr_{0.2}Co_{0.2}Fe_{0.8}O_{3-\delta}$ electrodes interfaced to CGO/YSZ. Solid State Ion 179:1080–1084. doi:10.1016/j.ssi.2008.02.028
36. Siebert E, Roux C, Boréave A, Gaillard F, Vernoux P (2011) Oxido-reduction properties of $La_{0.7}Sr_{0.3}Co_{0.8}Fe_{0.2}O_{3-\delta}$ perovskite oxide catalyst. Solid State Ion 183:40–47. doi:10.1016/j.ssi.2010.11.012
37. Bard AJ, Faulkner LR (2001) Electrochemical methods: fundamentals and applications, 2nd edn. Wiley & Sons, Inc., New York
38. Kournoutis VC, Tietz F, Bebelis S (2008) Cyclic voltammetry characterization of a $La_{0.8}Sr_{0.2}Co_{0.2}Fe_{0.8}O_{3-\delta}$ electrode interfaced to CGO/YSZ. Solid State Ion 197:13–17. doi:10.1016/574j.ssi.2011.06.007